Studying Slow Membrane Dynamics with Continuous Wave Scanning Fluorescence Correlation Spectroscopy

Jonas Ries and Petra Schwille
Technical University of Dresden, Dresden, Germany

ABSTRACT Here we discuss the application of scanning fluorescence correlation spectroscopy (SFCS) using continuous wave excitation to analyze membrane dynamics. The high count rate per molecule enables the study of very slow diffusion in model and cell membranes, as well as the application of two-foci fluorescence cross-correlation spectroscopy for parameter-free determination of diffusion constants. The combination with dual-color fluorescence cross-correlation spectroscopy with continuous or pulsed interleaved excitation allows binding studies on membranes. Reduction of photobleaching, higher reproducibility, and stability compared to traditional FCS on membranes, and the simple implementation in a commercial microscopy setup make SFCS a valuable addition to the pool of fluorescence fluctuation techniques.

INTRODUCTION

Fluorescence correlation spectroscopy (FCS) (1–3) is an established method for the determination of local concentrations, molecular weights, translational and rotational diffusion coefficients, chemical rate constants, association and dissociation constants, and photodynamics. First applied on molecules in solution, the use of FCS was then extended to the study of two-dimensional diffusion in artificial, supported lipid bilayers (4). Later, FCS was applied to native cell membranes and free-standing artificial lipid bilayers (5,6). The detection volume is usually positioned on a horizontal membrane, which can induce serious photobleaching: the slower the diffusion, the higher the residence time of the molecule in the detection volume. To avoid significant photobleaching of the fluorophores, which would lead to a distortion of the corresponding correlation curve, the excitation power has to be reduced. However, for reduced excitation powers, the dark counts of the detector will introduce additional noise in the correlation curve and the acquisition time has to be increased. To achieve a good signal/noise ratio, but also to avoid systematic distortions of the correlation curve due to short measurement times, continuous acquisition for time periods of several orders-of-magnitude larger than the diffusion times are required. But the long measurement times are limited by the stability of the setup. Changes of the position of the detection volume with respect to the membrane give rise to a distortion of the correlation curve and a poorly defined detection volume.

Various FCS-related methods with a scanning detection volume have been developed to circumvent some of the above-mentioned problems: Scanning FCS in solution (7–10) or on surfaces (11) can be used to study static and dynamic parameters of the system. Image correlation spectroscopy, first introduced by Petersen et al. (12), measures very slow dynamic parameters. Raster image correlation spectroscopy extends the application of this method to a wide range of diffusion times (13). Ruan et al. (14) introduced a new type of scanning FCS on membranes, which accesses the intermediate temporal regime. With this approach, the detection volume is scanned in a circular way through the equator of a giant unilamellar vesicle (GUV), which results in a set of correlation curves from all points along the scanned circle, permitting the study of binding and membrane dynamics which would otherwise be obscured by an excess of fluorophores in solution. Compared to FCS with a fixed detection volume at the top of the cell or vesicle, the alignment of the detection volume along the membrane in scanning fluorescence correlation spectroscopy (SFCS) allows for a better separation of the signal from fluorescent background in the solution. However, the use of two-photon excitation bears several risks due to the high photobleaching in membranes limiting the counts per particle and therefore, for a given acquisition time, the statistical accuracy of the correlation curve.

Here we discuss the use of one-photon scanning FCS as commonly applied in laser scanning microscopes and focus on studying membrane dynamics with high accuracy in challenging biological systems. The detection volume is scanned in a linear fashion (Fig. 1 *a*) rather than in the circular scan pattern employed in Ruan et al. (14). Furthermore, correlation curves were not calculated for all points along the scan path, but membrane movements are corrected for, and only the contributions of the membrane are taken into account to calculate the correlation curve. In this way we achieve a reproducible and well-defined detection volume even in an unstable system.

An important difference of the work presented here in comparison with that described in Ruan et al. (14) is the use of continuous wave excitation instead of two-photon excitation, which results in higher achievable counts per particle and reduced photobleaching. The improved signal not only permits shorter measurement times but also facilitates accurate measurements of very slow diffusion, encountered,

Submitted January 30, 2006, and accepted for publication May 12, 2006.

Address reprint requests to P. Schwille, Tel.: 49-351-4634-0328, E-mail: petra.schwille@biotec.tu-dresden.de.

0006-3495/06/09/1915/10 $2.00

doi: 10.1529/biophysj.106.082297

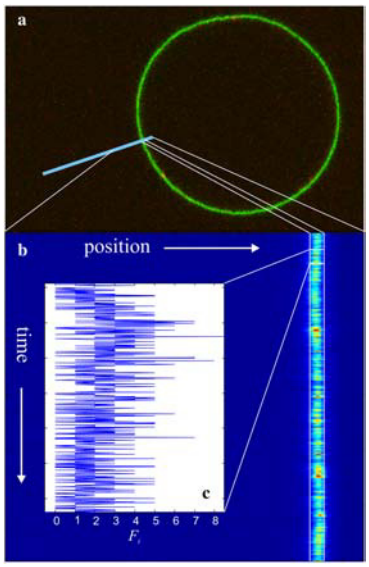

FIGURE 1 The principle of SFCS. (*a*) The detection volume is repeatedly scanned radially through the equator of the membrane. The linear scan path is chosen in such a way that the detection volume spends as little time as possible inside the GUV or cell to minimize out-of-focus photobleaching, which can lead to a depletion of fluorophores. (*b*) Each line scan is arranged as a row. The membrane can easily be identified and its contribution to each scan can be integrated to yield the intensity trace F_i (*c*).

for example, in yeast cell membranes. In addition, the enhanced signal allows for parameter-free determination of diffusion constants with two-foci cross-correlation spectroscopy (TFCCS) and binding studies using dual-color fluorescence cross-correlation spectroscopy (dcFCCS) with continuous and pulsed interleaved excitation.

Continuous wave SFCS can be easily implemented in a commercial laser scanning microscope and readily used with a modern FCS instrument like the Zeiss Confocor 3 (Carl Zeiss, Jena, Germany).

THEORY

Autocorrelation function for SFCS

In SFCS the detection volume is scanned perpendicularly through the equator of the membrane (Fig. 1 *a*), resulting in a transition time of the detection volume through the membrane much shorter than the diffusion time τ_D of the fluorophores. During data analysis, the emission, which can be attributed to the membrane-bound fluorophores, is integrated for each scan. These intensity values form the discrete time-trace F_i, which is used to calculate the correlation curve $G(\tau_i)$, where τ_i represents integer multiples of the scanning period T (Fig. 1).

For a fluorophore confined to the membrane ($x = 0$) at the position (y, z) and a scan in x-direction with a constant velocity v through all of the membrane, the average emitted light intensity is

$$I_e(y,z) = \frac{\varepsilon}{T}\int_{-t_m/2}^{t_m/2}\Omega(x(t),y,z)dt = \frac{\varepsilon}{vT}\int_{x(-t_m/2)}^{x(t_m/2)}\Omega(x,y,z)dx \approx \frac{\varepsilon}{vT}\int_{-\infty}^{\infty}\Omega(x,y,z)dx, \quad (1)$$

where t_m is the integration window, and $\varepsilon = \kappa Q I_0$ is the product of the setup efficiency κ, the fluorescence yield per fluorophore Q, and the excitation amplitude I_0. The value Ω is the molecule detection function of the setup, which is the product of excitation intensity distribution and the collection efficiency function of the objective-pinhole combination. Most commonly, a three-dimensional Gaussian is assumed for Ω:

$$\Omega(x,y,z) = \exp\left(-2\frac{(x^2+y^2)}{w_0^2} - 2\frac{z^2}{z_0^2}\right). \quad (2)$$

Then the emitted intensity in SFCS is described by a two-dimensional elliptical Gaussian:

$$I_e(y,z) \approx \frac{\varepsilon}{vT}\int_{-\infty}^{\infty}\Omega(x,y,z)dx = \sqrt{\frac{\pi}{2}}\frac{w_0\varepsilon}{vT}\exp\left(-2\frac{y^2}{w_0^2} - 2\frac{z^2}{z_0^2}\right). \quad (3)$$

This gives rise to the following autocorrelation function, describing two-dimensional diffusion of one component in a Gaussian elliptical detection volume:

$$G(\tau) = \frac{\langle I_e(\vec{r})P_D(\vec{r},\vec{r}',\tau)I_e(\vec{r}')\rangle}{c^2\langle I_e\rangle^2} = \frac{1}{N}\left(1+\frac{4D\tau}{w_0^2}\right)^{-1/2}\left(1+\frac{4D\tau}{w_0^2S^2}\right)^{-1/2}, \quad (4)$$

$$= \frac{1}{N}\left(1+\frac{\tau}{\tau_D}\right)^{-1/2}\left(1+\frac{\tau}{\tau_D S^2}\right)^{-1/2}. \quad (5)$$

$P_D(\vec{r},\vec{r}',\tau) = (c/4\pi D\tau)\exp(-(\vec{r}-\vec{r}')^2/4D\tau)$ is the number density autocorrelation function for two-dimensional diffusion for an average concentration c, $N = c\pi w_0 z_0$ is the mean number of molecules in the effective detection area, $\tau_D = (w_0^2/4D)$ is the diffusion time, and the structure parameter $S = z_0/w_0$ describes the ellipticity of the detection area.

The triplet contribution has been neglected since triplet times are in the range of microseconds and cannot be resolved with SFCS.

Two-foci cross correlation (TFCCS)

By alternately scanning along two lines at a distance d parallel to each other, two effective foci in the membrane with a displacement d along the y-direction can be realized (Fig. 2 *a*). The photons in the two foci are not collected within the same time window, but with a delay t_d, which is usually given by the scan period. If t_d is much smaller than the diffusion time τ_D, it can be neglected. The cross correlation of the intensity traces corresponding to the two intersections results in the correlation curve (15,16)

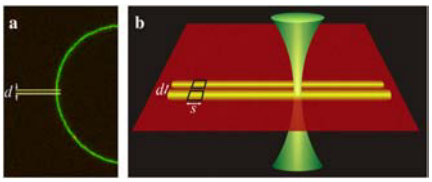

FIGURE 2 The principle of scanning two-foci cross correlation. (*a*) TFCCS in vertical membranes. Two lines with a separation of d are repeatedly scanned through the equator of a GUV. Each intersection with the membrane gives rise to a fluorescence burst, and fluorescent bursts from all passes through the membrane are connected to an intensity trace. (*b*) TFCCS in planar membranes: Two lines with a separation d are scanned in the membrane. Intensity traces are extracted from corresponding parts (equivalent time windows) of the two scans (*boxes*).

$$G_x(\tau) = \frac{1}{N}\left(1+\frac{\tau}{\tau_D}\right)^{-1/2}\left(1+\frac{\tau}{\tau_D S^2}\right)^{-1/2}\exp\left(-\frac{d_r^2}{1+\tau/\tau_D}\right), \tag{6}$$

where $d_r = d/w_0$ is the distance of the foci in units of the radius of the detection volume. The use of direct physical parameters D and w_0 results in

$$G_x(\tau) = \frac{1}{N}\left(1+\frac{4D\tau}{w_0^2}\right)^{-1/2}\left(1+\frac{4D\tau}{w_0^2 S^2}\right)^{-1/2} \exp\left(-\frac{d^2}{w_0^2+4D\tau}\right). \tag{7}$$

The cross-correlation curve shows a maximum at a specific lag time, which is given by the characteristic time it takes a fluorophore to diffuse from one detection area to the other.

Once d is known, D and w_0 can be determined directly by fitting the data to Eq. 7 without any additional calibration measurement. A global fit of the two autocorrelation functions and the cross-correlation function improves the accuracy.

Because of the alternating data collection in the two foci, the resulting cross-correlation curve is shifted by the delay time t_d, as can be seen by looking at the definition of the cross-correlation curve G_x for intensity traces $F(t)$ and $H(t)$ and the cross-correlation curve G_x^d for intensity traces $F(t)$ and $H(t + t_d)$:

$$G_x(\tau) \propto \int F(t)H(t+\tau)dt$$
$$G_x^d(\tau) = G_x(\tau+t_d) \propto \int F(t)H(t+t_d+\tau)dt. \tag{8}$$

If t_d is not much smaller than τ_D, this shift needs to be taken into consideration in performing the fit.

Two-foci cross correlation on planar membranes

The same setup also permits TFCCS on planar membranes with the additional advantage of simultaneous determination of diffusion coefficients in different parts of the sample. As depicted in Fig. 2 *b*, two parallel lines are scanned within the membrane and the contributions from corresponding parts of the sample (denoted by a box) of the length s belonging to the equivalent time window $t_m = s/v$ are summed up for each scan. Depending on the length of the time window, the effective detection area can be practically circular (very short time window) or a line (long time window).

The unnormalized molecule detection function $\Omega(x, y)$ is given by the convolution of the Gaussian detection area of waist radius w_0 with a step function of length s, describing the scanning in x direction:

$$\Omega(x,y) = \int_0^s \exp\left(-2\frac{y^2+(x-x')^2}{w_0^2}\right)dx' = \sqrt{\frac{\pi}{8}}w_0\exp\left(-\frac{2y^2}{w_0^2}\right)\left(\mathrm{erf}\left(\frac{\sqrt{2}(s-x)}{w_0}\right) + \mathrm{erf}\left(\frac{\sqrt{2}x}{w_0}\right)\right). \tag{9}$$

The cross-correlation function for two detection areas at a distance d can then be calculated as

$$G_x(\tau) = \frac{\iiiint \Omega(x,y)P_D(x,y,x',y')\Omega(x',y'-d)\,dxdydx'dy'}{c^2\left(\iint \Omega(x,y)dxdy\right)^2} \tag{10}$$

$$= \frac{1}{c\pi s^2}\exp\left(-\frac{d^2}{w_0^2+4D\tau}\right) \times\left[\frac{\sqrt{\pi}s}{\sqrt{w_0^2+4D\tau}}\mathrm{erf}\left(\frac{s}{\sqrt{w_0^2+4D\tau}}\right) + \exp\left(-\frac{s^2}{w_0^2+4D\tau}\right)-1\right]. \tag{11}$$

The autocorrelation curve follows from Eq. 11 for $d = 0$.

An elongated detection volume offers the advantage of a high signal/noise ratio in the correlation curve, since one out of two fluorophores that originates in one detection area will finally reach the second one.

Dual-color cross correlation

In dual-color cross correlation (dcFCCS) the auto- and cross-correlation curves for two spectral channels are calculated. In case of an ideal setup with completely overlapping detection volumes V_{eff} and negligible spectral cross talk, the concentrations of the unbound molecules c_a and c_b and of the bound molecules c_{ab} can be determined from the amplitudes of the correlation functions (17):

$$G_a(0) = \frac{1}{V_{eff}(c_a+c_{ab})}, \quad G_b(0) = \frac{1}{V_{eff}(c_b+c_{ab})}$$
$$G_{ab}^x(0) = \frac{c_{ab}}{V_{eff}(c_a+c_{ab})(c_b+c_{ab})}. \tag{12}$$

In case of a nonperfect overlap of the detection volumes, Eq. 6 describes the cross-correlation function. Yet, for small

imperfections, Eq. 5 can be used to fit the data and Eq. 12 can be used approximately if one compares the measured cross-correlation amplitude to the maximally achievable cross-correlation amplitude. The maximally achievable cross-correlation amplitude corresponds to a complete binding of the species involved and can be estimated using a sample with known high cross correlation (16). Often a double-labeled molecule (i.e., DNA) with a high labeling efficiency is used.

MATERIALS AND METHODS

Optical setup

Confocal imaging and scanning FCS measurements were performed on a LSM Meta 510 system (Carl Zeiss, Jena, Germany) using a 40 × NA 1.2 UV-VIS-IR C-Apochromat water immersion objective and a home-built detection unit at the fiber output channel: A bandpass filter was used behind a collimating achromat lens to reject the residual laser and background light. Another achromat (LINOS Photonics, Göttingen, Germany) with a shorter focal length was used to image the internal pinhole onto the aperture of the fiber of the avalanche photo diode (Perkin-Elmer, Boston, MA). The photon arrival times were recorded in the photon mode of the hardware correlator Flex 02-01D (correlator.com, Bridgewater, NJ). For dual-color measurements, a dichroic mirror, placed behind the collimating achromat, was used to separate the two channels. Each channel contained a suitable emission filter and an achromat to image the internal pinhole onto the aperture of the fiber of the corresponding avalanche photo diode. All filters and dichroic mirrors, as specified in Results, were purchased from AHF Analyze Technik (Tuebingen, Germany).

The movement of the detection volume was controlled directly with the Zeiss LSM operation software. The line mode was used for one-focus measurements and the frame mode with $N \times 2$ pixels for two-foci measurements. For pulsed interleaved excitation (PIE) the multitrack mode was applied. In this mode the excitation lasers are alternately used for every other line scan by blocking the undesired laser line with an acousto-optical tunable filter. Bidirectional scanning was employed whenever useful to increase the acquisition speed.

The distance d between the two lines for two-foci FCS was measured by repeatedly scanning over a film of dried fluorophores and measuring the distance between the bleached traces in a high resolution LSM-Image.

All measurements were performed at room temperature (22°C).

Materials

1,2-dioleoyl-*sn*-glycero-3-phosphocholine (dioleoylphosphatidylcholine; DOPC), *n*-stearoyl-*d*-erythrosphingosylphosphorylcholine (sphingomyelin), and cholesterol were purchased from Avanti Polar Lipids (Alabaster, AL) and used without further purification. Lissamine rhodamine B 1,2-dihexadecanoyl-*sn*-glycero-3-phosphoethanolamine triethylammonium salt (Rhodamine DHPE), BODIPY FL C5-ganglioside GM1 (GM1-BODIPY-FL), cholera toxin subunit B (recombinant), Alexa Fluor 488 conjugate (ctxB-Alexa488), 1,1′-dioctadecyl-3,3,3′,3′-tetramethylindocarbocyanine perchlorate ($DiIC_{18}$, DiI), and 3,3′-dioctadecyloxacarbocyanine perchlorate ($DiOC_{18}$, DiO) were purchased from Molecular Probes (Eugene, OR). Ganglioside GM1, Bovine Brain, was purchased from Merck KGaA (Darmstadt, Germany). Cholera toxin subunit B, labeled with Cy5 (ctxB-Cy5), was produced according to Bacia et al. (18).

Yeast cells expressing Fus-Mid-GFP from a centromeric plasmid pTPQ55 were a kind gift of Kai Simons (MPI-CBG, Dresden, Germany). To reduce intracellular staining we used a *vps1*Δ mutant (for details see (19)).

Preparation of model membranes

Giant unilamellar vesicles were produced by a modified electroformation method as described previously (20), using a custom-made closed perfusion chamber heated to 65°C and indium-tin-oxide coated coverslips as electrodes. Briefly, a 5-μL lipid mixture, as indicated in Results, was deposited on indium-tin-oxide-coated coverslips. After evaporation of the solvent, the chamber was assembled and filled with water. A voltage of 1.2 V at 10 Hz was applied for ~2 h. Where applicable, labeled ctxB was added at a saturating concentration to the flow chamber after GUV formation and incubated for 10 min at room temperature. The optical setup was adjusted to the labeled ctxB in solution in the chamber. Residual ctxB was removed by applying a slow flow of water through the perfusion chamber.

Planar supported bilayers were prepared as follows (21): DOPC (molar concentration 80%), Cholesterol (20%), and Rhodamine DHPE (0.001%) were dissolved in chloroform and evaporated under nitrogen flux and then under vacuum for 1 h. The lipids were then rehydrated with 150 mM NaCl, 10 mM HEPES buffer (pH 7.4) and resuspended by vigorous vortexing. The suspension was bath-sonicated at 60°C for 1 h to obtain small unilamellar vesicles. Ten microliters were then placed on a freshly cleaved mica substrate glued to a glass coverslip, for 30 min at room temperature. After that, the sample was rinsed several times to remove unfused vesicles.

Data analysis

Data analysis was performed with software written in MatLab (The MathWorks, Natick, MA). The photon stream was binned in bins of 100 ns to 5 μs depending on the scan speed and arranged as a matrix such that every row corresponded to one line scan (Fig. 1 *b*). Movements of the membrane were corrected-for by calculating the position of the maximum of a running average over several hundred line scans and shifting it to the same column. An average over all rows was fitted with a Gaussian and only the elements of each row between $-2.5\ \sigma$ and $2.5\ \sigma$ were added to construct the intensity trace. The correlation function of the resulting intensity trace F_i was computed with a multiple-tau correlation algorithm (22). The correlation curves were fitted with a weighted nonlinear least-squares fitting algorithm. Errors given in the figures are the 95% confidence intervals on the nonlinear least-squares parameter estimates; errors indicated in the text take into account the uncertainties of additional parameters, such as the waist radius w_0 or the distance between foci d.

For two-foci measurements, two intensity traces F_i and H_i were extracted from the photon stream and processed in an analogous way. Equations 4 and 7 were fitted globally to obtain one set of fit parameters.

For dcFCCS with continuous excitation, one intensity trace was extracted from each channel as described above and auto- and cross-correlation curves were calculated and fitted to Eq. 5 to determine relative cross-correlation amplitudes. For dcFCCS with PIE, two intensity traces were extracted from the orange channel and one from the green channel (cross excitation of the green dye with the orange laser and cross talk of the orange dye into the green channel were negligible).

RESULTS

Scanning FCS of slowly diffusing molecules

Fig. 3 shows the SFCS autocorrelation curve of ctxB-Alexa488 bound to a GUV with a lipid composition of 25% cholesterol, 75% sphingomyelin, and 0.005% GM1, chosen to ensure slow diffusion. Details are given in the figure legend. The waist radius was determined in a solution of fluorophores to be $w_0 = 200 \pm 20$ nm. Based on this, the diffusion time of $\tau_D = 524 \pm 54$ ms corresponds to a diffusion coefficient of $D = 0.019 \pm 0.006\ \mu m^2/s$.

Two-foci cross correlation in GUVs

For two-foci cross correlation (TFCCS), two parallel lines were scanned through the equator of a GUV (Fig. 2 *a*)

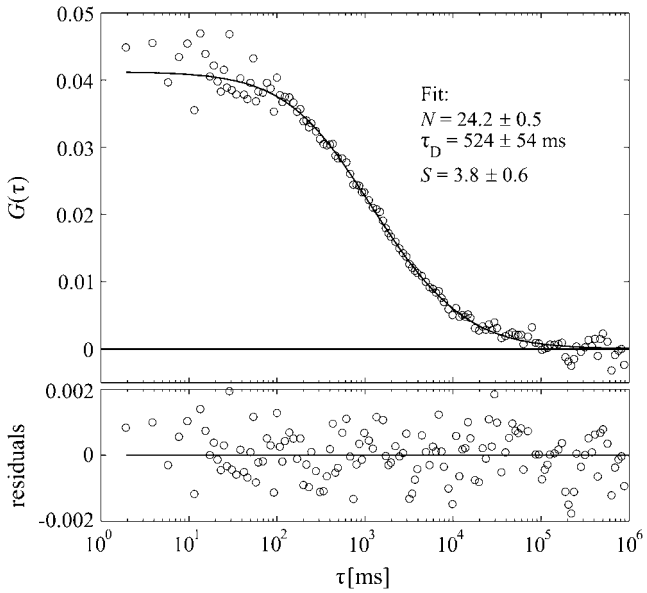

FIGURE 3 SFCS autocorrelation curve (○) of ctxB-Alexa488 bound to a GUV composed of 25% cholesterol, 75% sphingomyelin, and 0.005% GM1 with corresponding fit to Eq. 6 (—) and weighted residuals. Measurement parameters: Acquisition time: 20 min, excitation power $P = 3.75\ \mu$W at 488 nm, repetition rate $f = 520$ Hz, and scan speed $v = 0.14$ m/s. Integration time for the membrane contribution is $t_m = 5.5\ \mu$s; average number of photons in each line scan is $\langle F_i \rangle = 0.42$. Emission filter is HQ525/60 M; pinhole is 60 μm.

composed of 32% cholesterol, 68% sphingomyelin, and 0.003% GM1, labeled with ctxB-Alexa488. The corresponding auto- and cross correlation curves of the two resulting foci are shown in Fig. 4 *a*. The drop in the cross-correlation curve for small lag times is clearly visible. It is preferable to fit the data directly to Eq. 7 instead of Eq. 6, since the physical quantities of interest, w_0 and D, are independent, whereas d_r and τ_D exhibit a higher degree of correlation. The distance d between the two lines was determined to be 300 ± 15 nm as described in Materials and Methods. A global fit of the measured correlation curves to Eq. 7 resulted in $w_0 = 199 \pm 12$ nm and $D = 0.23 \pm 0.03\ \mu m^2/s$. Due to the different composition of the GUV, this value is an order-of-magnitude higher than the diffusion coefficient measured in the previous section.

For a comparison, Fig. 4 *b* shows the autocorrelation curve obtained with one-focus SFCS on a GUV with the same composition as above. The diffusion time of $\tau_D = 42 \pm 3$ms corresponds to a diffusion coefficient of $D = 0.24 \pm 0.07\ \mu m^2/s$, based on a waist radius of $w_0 = 200 \pm 20$ nm determined from a calibration measurement of Alexa488 in solution.

Two-foci cross correlation on planar membranes

Fig. 5 shows the outcome of scanning TFCCS on a homogeneous supported lipid bilayer, as described in Theory, above, and Fig. 2 *b*. The bilayer was composed of 80% DOPC and 20% cholesterol and was labeled with 0.001% Rhodamine DHPE. The two lines had a separation of $d = 430 \pm 20$ nm. The length of the part of the line scan used to construct the intensity trace was $s = 2.87\ \mu$m. The resulting diffusion coefficient $D = 3.5 \pm 0.3\ \mu m^2/s$ is in good agreement with a value of $D = 4.1 \pm 0.8\ \mu m^2/s$ obtained with traditional FCS.

Dual-color cross correlation

To demonstrate the potential of SFCS for dual-color cross-correlation analysis (dcFCCS), we incorporated fluorescent GM1-BODIPY-FL into GUVs composed of 50% cholesterol and 50% sphingomyelin. Ten micrograms of ctxB-Cy5, which binds specifically to up to five GM1 molecules, was injected in the perfusion chamber and residual ctxB-Cy5 was removed after 10 min. Spectral cross talk of the fluorophores into the other channel was negligible. Fig. 6 shows the resulting auto- and cross-correlation curves together with fits to Eq. 5. The relative cross-correlation amplitude is 30%.

Dual-color cross correlation with pulsed interleaved excitation

Spectral cross talk can lead to a false-positive cross correlation, which can be avoided by using pulsed interleaved excitation (PIE) (23). Usually alternating short laser pulses with a repetition rate of several MHz are required for PIE. In SFCS, PIE can be implemented in a much simpler fashion. By alternating the green and the orange excitation for every other line scan, the contributions from the different fluorophores can be separated. This is due to the fact that the contributions from the green-emitting fluorophores in the orange detection channel upon excitation with the orange laser, and that from the orange-emitting fluorophores in the green detection channel upon excitation with the green laser, are negligible. Fig. 7 *a* shows auto- and cross-correlation curves obtained on GUVs composed of 50% cholesterol and 50% sphingomyelin and labeled with 0.004% DiO and 0.002% DiI. These two dyes are not supposed to cross-correlate and have partially overlapping excitation and emission spectra. Fig. 7 *b* shows the auto- and cross-correlation curves obtained on the same sample as Fig. 7 *a* using PIE.

SFCS in yeast cells

Fig. 8 *a* shows the result of a one-focus SFCS measurement on Fus-Mid-GFP in yeast cell membranes. The diffusion coefficient was determined to be $D = 0.0028 \pm 0.0011\ \mu m^2/s$, based on a waist radius of the detection volume of $w_0 = 150 \pm 15$ nm, previously determined with free dye in solution. Fig. 8 *b* shows a two-foci measurement on the same protein. The diffusion coefficient was found to be $D = 0.0026 \pm 0.0006\ \mu m^2/s$, and the distance between the foci was previously determined to be $d = 300 \pm 15$ nm.

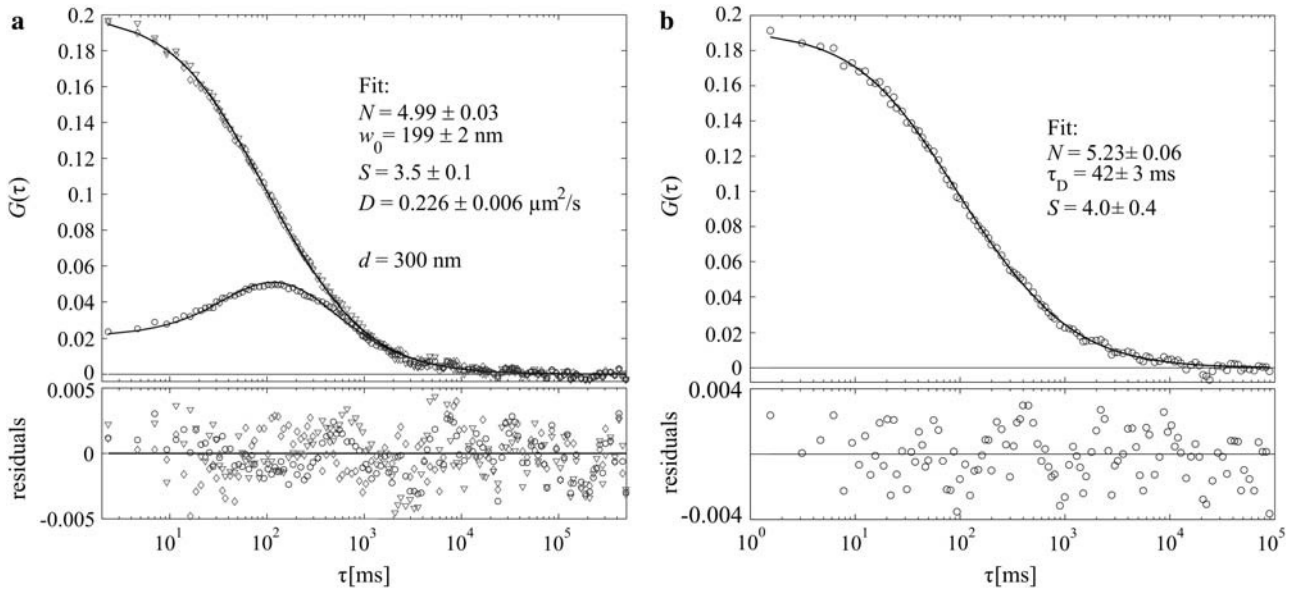

FIGURE 4 (*a*) Scanning two-foci cross correlation. Auto- ($\diamond$,∇) and cross-correlation curves ($\bigcirc$) for SFCS with two distinct lines with a separation of $d = 300 \pm 15$ nm and residuals from the global fit to Eqs. 4 and 7 (—). Composition of the GUV: 32% cholesterol, 68% sphingomyelin, and 0.003% GM1, labeled with ctxB-Alexa488. Measurement parameters: Acquisition time is 20 min, excitation power $P = 6.1$ μW at 488 nm, repetition rate $f = 430$ Hz, scan speed $v = 0.046$ m/s, and integration time $t_m = 27$ μs. Emission filter is HQ525/60 M; pinhole is 60 μm. (*b*) Autocorrelation curve ($\bigcirc$) obtained with one-focus SFCS on a GUV of the same composition as above with corresponding fit to Eq. 5 (—) and weighted residuals. Measurement parameters: Acquisition time: 15 min, excitation power $P = 6.1$ μW at 488 nm, repetition rate $f = 640$ Hz, scan speed $v = 0.07$ m/s, and integration time $t_m = 9$ μs. Emission filter is HQ525/60 M; pinhole is 60 μm.

DISCUSSION

Scanning FCS of slowly diffusing molecules

The measurement of slow diffusion in membranes requires long acquisition times in order to average over a sufficiently high number of independent events. For continuous illumination the excitation power has to be low to avoid photobleaching, which results in a low signal hardly distinguishable from the background. The signal/noise ratio can be greatly increased by using pulsed excitation with short (μs) pulses of high power followed by long (millisecond) pauses, as implemented here by scanning the detection volume through the membrane. The excellent signal/noise ratio of SFCS was demonstrated in GUVs with slowly diffusing fluorophores (Fig. 3): Since the detection volume spent only a small fraction of the total acquisition time in the membrane, the resulting average excitation intensity in the membrane was greater than two-orders-of-magnitude below the excitation intensity and ensured negligible photobleaching. The resulting average count rate was only 0.22 kHz (corresponding to 0.01 kilo counts per particle per second (kcpps)), which was comparable to the rate of dark counts from the detector. However, the count rate during the transition time t_m was 75 kHz (3.3 kcpps).

Another important advantage of SFCS is its robustness to instabilities which limit the acquisition times in static FCS on membranes. In SFCS, slow movements are corrected-for and the contributions from all of the membrane are summed up. As a result, a reproducible and well-defined detection area is obtained, and the measurement becomes insensitive to membrane undulations, which can otherwise be a severe problem since they mimic an additional diffusing component (24).

To calculate the diffusion coefficient from the diffusion time, the waist w_0 of the detection area has to be known. It can be determined by calibration measurements with free dye or with two-foci SFCS. It can also be extracted directly from the line scans (Fig. 1 *b*) by fitting the line profile to a Gaussian, but nonperpendicular scanning, residual curvature, or faster membrane movements result in an enlarged estimate for this value.

In one-focus measurements, an exact calibration of the detection area is complicated, since varying alignment, temperature, refractive index of the sample, or cover-slide thickness result in a poorly defined detection volume (25). Moreover, calibration measurements performed in solution to determine the two-dimensional detection area on the membrane are only exact for an ideal Gaussian detection volume.

Two-foci cross correlation

With scanning two-foci FCS (TFCCS) we measured absolute diffusion coefficients without the need for calibrating the detection area (Fig. 4 *a*). The one-focus measurement (Fig. 4 *b*) resulted in a similar value for the diffusion coefficient, but the error was significantly higher due to the difficulties of determining the detection area. The advantage of two-foci

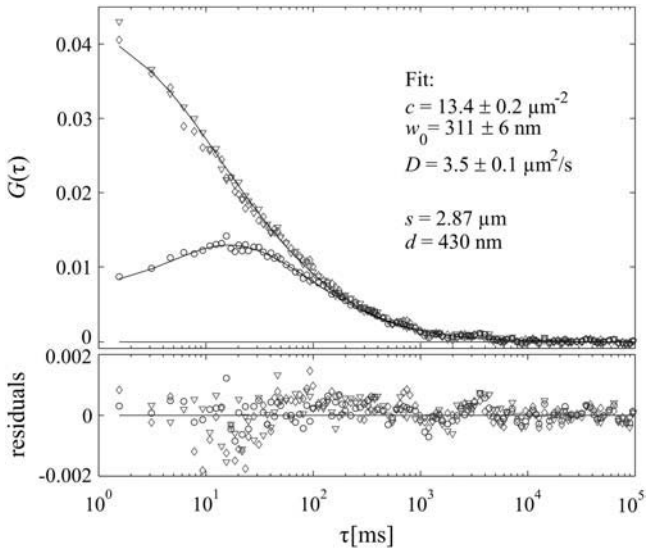

FIGURE 5 Scanning two-foci cross correlation on a supported lipid bilayer. Auto- (◇,∇) and cross-correlation curves (○) for SFCS with two distinct lines of length $s = 2.87\ \mu$m with a separation of $d = 430 \pm 20$ nm and residuals from the global fit to Eq. 11 (—). Composition of the membrane: 80% DOPC, 20% cholesterol, and 0.001% Rhodamine DHPE. Measurement parameters: Acquisition time is the average over three acquisitions of 4 min each, excitation power $P = 50\ \mu$W at 543 nm, repetition rate $f = 643$ Hz, scan speed $v = 0.07$ m/s, and integration time $t_m = 41\ \mu$s. Emission filter is HQ585/40 M; pinhole is 80 μm.

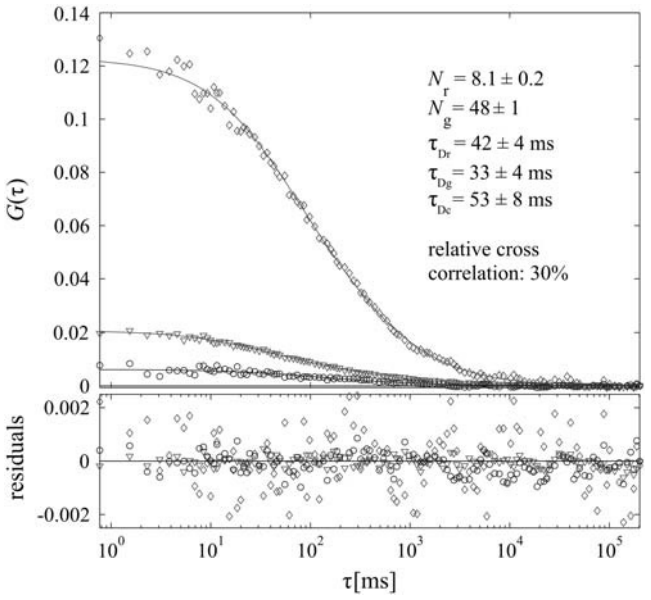

FIGURE 6 Scanning dual-color cross correlation. Auto- (*red channel*, ◇; *green channel*, ∇) and cross-correlation curves (○) for dual-color cross correlation and weighted residuals from the fit to Eq. 5 (—). Composition of the GUV: 50% cholesterol, 50% sphingomyelin, and 0.004% GM1-BODIPY-FL. Incubated with 10 μg ctxB-Cy5. Measurement parameters: Acquisition time is the average over four acquisitions of 6 min each, excitation powers $P = 4.8\ \mu$W at 488 nm and $P = 8.0\ \mu$W at 633 nm, repetition rate $f = 1.3$ kHz, scan speed $v = 0.07$ m/s, and integration time $t_m = 20\ \mu$s. Emission filters are HQ525/60 M and HQ700/75 M, dichroic mirror is 610DCXR, and pinhole is 65 μm.

SFCS versus one-focus SFCS is even greater for small diffusion times comparable to the scanning period, where meaningful fitting of the autocorrelation curve is limited. By choosing an appropriate distance d, the maximum of the cross-correlation curve can be shifted into the measurement window, rendering accurate fitting possible.

The application of TFCCS is not restricted to spherical membranes. It can also be applied to determine absolute diffusion coefficients on planar membranes (Fig. 5). Since drifts of the setup cannot be corrected-for any longer, SFCS on planar membranes is sensitive to instabilities. However, positioning of the detection volume is no longer crucial, since the waist radius can be determined directly from the fit and does not enter the determination of the diffusion coefficient. Moreover, the length s of the detection area can be easily inferred from the data set, which reduces the number of fit parameters by one, compared to measurements on vertical membranes, rendering the results of the fit more reliable.

Dual-color cross correlation

Scanning dual-color cross correlation (dcFCCS) permits the study of binding and aggregation of labeled molecules on the membrane without the risk of false-positive cross correlation due to membrane movements. Fig. 6 shows auto- and cross-correlation curves of GM1-BODIPY-FL incorporated into a GUV and ctxB-Cy5, which binds to up to five GM1 molecules. Spectral cross talk was negligible. The amplitudes of the autocorrelation curves indicate that the concentration of labeled GM1 molecules is substantially higher than the concentration of ctxB molecules, which could be consistent with unbound GM1 in the inner leaflet of the membrane and GM1 bound to ctxB in the outer leaflet. The relative cross-correlation amplitude is 30%. A calibration measurement on double-labeled DNA molecules in free solution used as a cross-correlation reference showed a cross-correlation amplitude of 55%. For a ratio of bound complexes to unbound GM1 of 1:5 in the absence of quenching or FRET, a relative cross-correlation amplitude of $1.66 \times 55\%$ can be expected (16,26). The reduced cross-correlation amplitude could result from a loss of fluorescence of the GM1-BODIPY-FL due to photobleaching or self-quenching, inhomogeneous labeling of the ctxB, and a deteriorated overlap of the detection areas due to the different optical geometry in SFCS.

Dual-color cross correlation with pulsed interleaved excitation

If spectrally closer dyes are used, spectral cross talk, especially from the green dye into the red channel, can lead to a false-positive cross-correlation amplitude. This can be seen in Fig. 7 *a*, obtained on GUVs labeled with DiO and DiI, which have partially overlapping excitation and emission

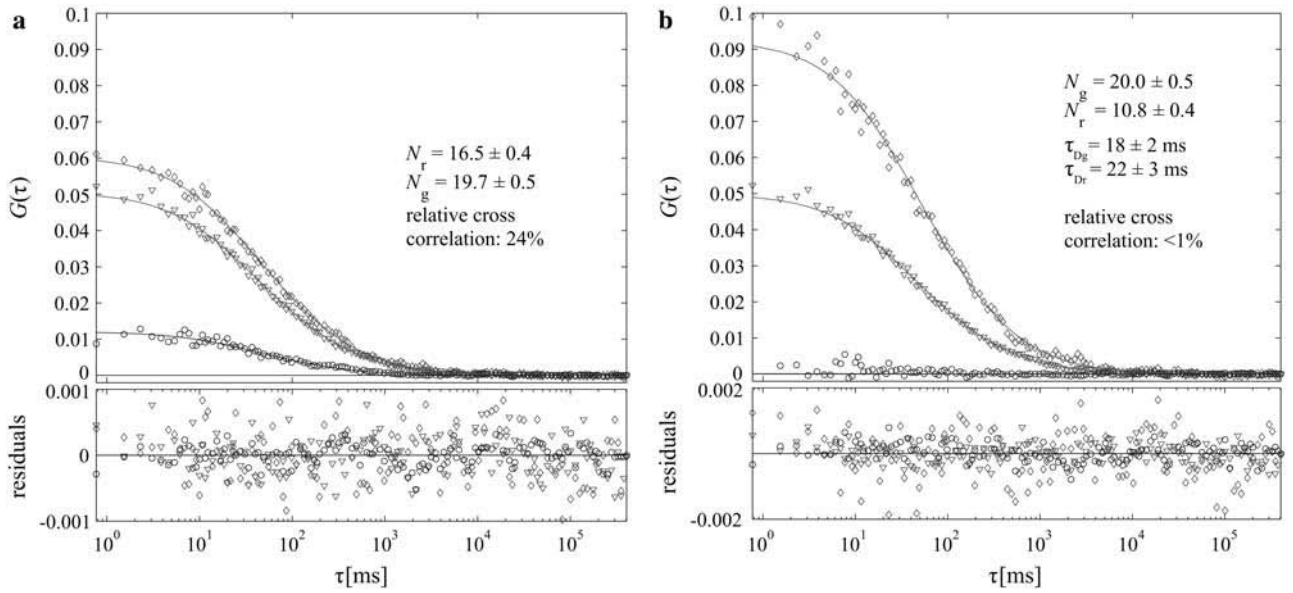

FIGURE 7 dcFCCS with PIE. Auto- (*orange channel*, ◇; *green channel*, ∇) and cross-correlation curves (○) for dual-color cross correlation without and with PIE and weighted residuals from the fit to Eq. 6 (—). Composition of the GUV: 50% cholesterol, 50% sphingomyelin, 0.004% DiO, and 0.002% DiI. Measurement parameters: Acquisition time is the average over four acquisitions of 10 min each, alternate scanning with excitation powers $P = 6.2$ μW at 488 nm and $P = 2.0$ μW at 543 nm, repetition rate $f = 1.3$ kHz, scan speed $v = 0.10$ m/s, and integration time $t_m = 20$ μs. Emission filters are HQ515/30 M, HQ585/40 M, dichroic mirror is D555, and pinhole is 65 μm. For panel *a*, contributions from both the green and the orange excitation in the orange channel were summed up resulting in an effective simultaneous excitation. For panel *b*, only contributions from the orange excitation were included in the intensity trace of the orange channel, which effectively eliminates cross talk. The signal from orange excitation in the green channel was negligible.

spectra. Here the relative cross-correlation amplitude due to cross talk was as large as 25%.

Fig. 7 *b* shows the auto- and cross-correlation curves from the same sample as Fig. 7 *a*, making use of PIE. The amplitude of the orange autocorrelation curve is significantly higher since it is now free of cross talk. Most importantly, the cross-correlation amplitude completely vanishes, indicating good separation of the dyes.

PIE can be easily applied in scanning dcFCCS without any additional hardware in a confocal microscope by using the multitrack mode. In addition to avoiding cross talk, PIE allows for quantitative analysis of FRET between the two labeled species (27) and an accurate overlap of the detection volumes can more easily be achieved.

SFCS on yeast cell membranes

Due to its high intrinsic stability and optimal separation of membrane and bulk contributions, SFCS permits dynamic measurements even on yeast cell membranes. Previously, it was only possible to assess this kind of extremely slow membrane diffusion using fluorescence recovery after photobleaching (28). Fig. 8 *a* shows the result of a one-focus SFCS measurement on Fus-Mid-GFP in yeast cell membranes. Because the measurement time was only ~100-fold longer than the diffusion time, the correlation curve had to be fit with an offset (29). The resulting diffusion coefficient of $D = 0.0028 \pm 0.0011$ $\mu m^2/s$ is comparable with the results of fluorescence-recovery-after-photobleaching measurements on GFP-Snc1p (28).

The diffusion coefficient determined by a two-foci measurement (Fig. 8 *b*, $D = 0.0026 \pm 0.0006$ $\mu m^2/s$) is consistent with that value. The measurement time was the same as for Fig. 8 *a*. Although the curves look slightly more noisy, the diffusion coefficient was actually determined with a higher accuracy, thanks to the additional information from the spatial cross correlation.

SFCS versus traditional FCS

SFCS expands the application of FCS to larger diffusion times. For fast diffusion in membranes, traditional FCS can be superior once the detection volume has been carefully calibrated: It allows for shorter measurement times, easy data analysis, minimized out-of-focus photobleaching, and submicrosecond time resolution. In SFCS, the time resolution is limited by the scanning frequency to approximately a millisecond. Yet in this regime scanning two-foci measurements can lead to far more accurate determination of absolute diffusion constants.

The lower limit for diffusion coefficients measurable with SFCS is determined by the measurement time. The maximum measurement time is limited by drifts of the vesicle perpendicular to the scan direction, which will lead to a scan path nonperpendicular to the membrane and therefore to a distortion of the detection area. In addition, the drift will

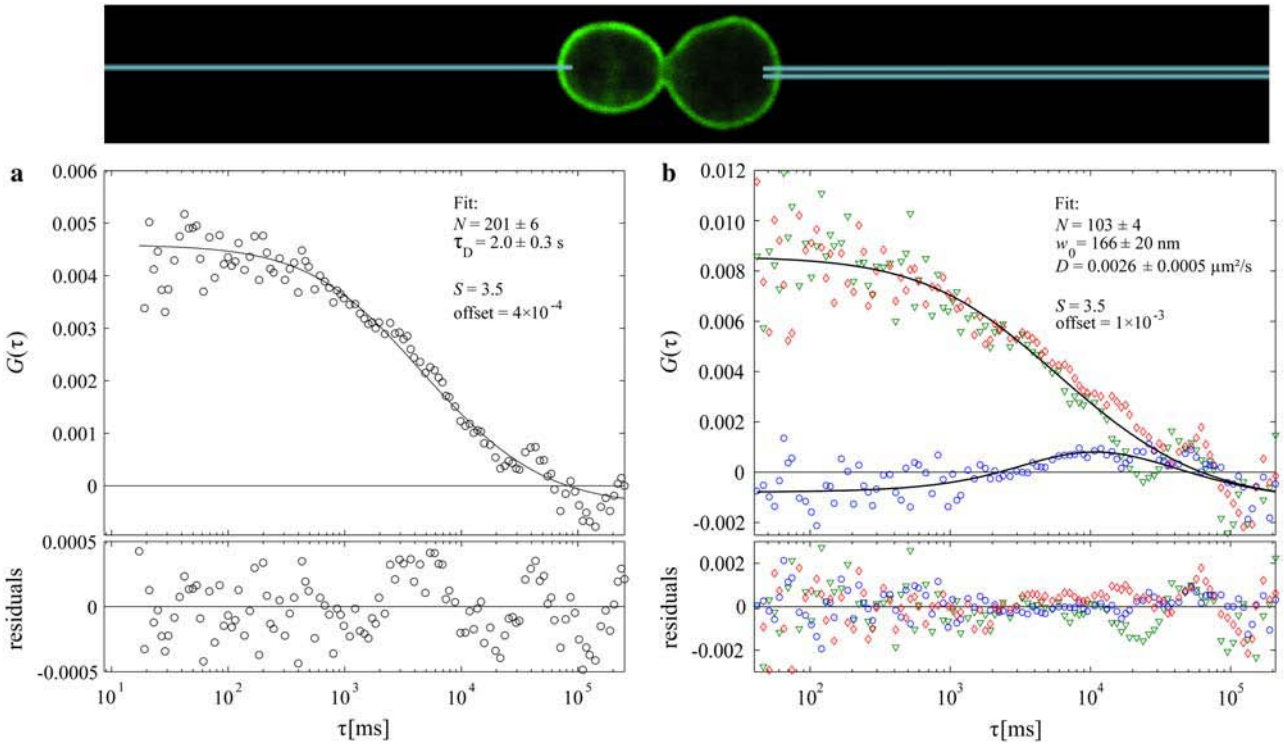

FIGURE 8 SFCS measurements on Fus-Mid-GFP in yeast cell membrane. (*a*) Autocorrelation curve (○) and weighted residuals from the fit to Eq. 5 (—). Measurement parameters: Acquisition time is 6 min, excitation power $P = 1.2$ μW at 488 nm, repetition rate $f = 1.04$ kHz, scan speed $v = 0.09$ m/s, and integration time $t_m = 9$ μs. Emission filter is HQ525/60 M; pinhole is 60 μm. (*b*) Auto- (◇,∇) and cross-correlation curves (○) and residuals from the global fit to Eqs. 4 and 7 (—). Measurement parameters: Acquisition time is 6 min, excitation power $P = 1.2$ μW at 488 nm, repetition rate $f = 434$ Hz, scan speed $v = 0.046$ m/s, integration time $t_m = 27$ μs, and $d = 300 \pm 15$ nm. Emission filter is HQ525/60 M; pinhole is 60 μm.

contribute to the correlation curves as an additional flow term. For large vesicles we found measurement times of up to 1 h to be practical, resulting in a smallest measurable diffusion coefficient being on the order of 10^{-3} μm^2/s.

One important drawback of SFCS with a scan path perpendicular to the membrane is the requirement of a vertical membrane, which precludes its use on flat substrate-adherent cells. However, if stability is not a limiting factor, SFCS can be readily applied on horizontal membranes.

CONCLUSION

We have demonstrated the capacity of continuous wave scanning FCS for accurate diffusion and binding studies on membranes. The intrinsic robustness to instability, the excellent signal/noise ratio, and negligible photobleaching allowed for long uninterrupted acquisition times, which are essential for measuring slow diffusing molecules.

The extension to two-foci spatial cross correlation enabled us to perform direct and accurate measurements of diffusion coefficients without the need for calibrating the detection volume. Two-foci scanning cross-correlation spectroscopy was also successfully applied on planar membranes enabling simultaneous, calibration-free measurements of diffusion times in different parts of the sample. The extension to study slow three-dimensional diffusion in solution or inside cells is straightforward.

Scanning dual-color cross-correlation spectroscopy permits quantitative binding and aggregation studies on membranes without the risk of false-positive cross correlation due to membrane movements. The implementation of PIE was shown to successfully eliminate spectral cross talk, permitting the choice of spectrally close fluorophores and providing the prospect of quantitative FRET measurements on membranes using FCS (27).

The high intrinsic stability, the excellent signal/noise ratio, and the good separation of membrane and bulk contributions of SFCS enabled the study of diffusion on yeast cell membranes, which was previously impossible with FCS due to extremely slow diffusion in the range of 10^{-3} μm^2/s.

The various approaches to continuous wave scanning FCS demonstrated here allow the study of different aspects of membrane dynamics on a variety of systems with an accuracy unprecedented in traditional FCS. The simple implementation in a commercial setup should help SFCS to become a standard technique for membrane studies.

We thank Salvatore Chiantia for preparation of the planar-supported bilayers, Lawrence Rajendran and Robin Klemm for providing and preparing the cells, Kirsten Bacia for preparation of ctxB-Cy5, and Zdenek Petrasek, Kirsten Bacia, and Madhavi Krishnan for help with the manuscript.

This work was supported by Europaeischer Fond fuer Regionale Entwicklung grant No. 4212/04-02.

REFERENCES

1. Magde, D., W. W. Webb, and E. Elson. 1972. Thermodynamic fluctuations in a reacting system—measurement by fluorescence correlation spectroscopy. *Phys. Rev. Lett.* 29:705.
2. Eigen, M., and R. Rigler. 1994. Sorting single molecules: application to diagnostics and evolutionary biotechnology. *Proc. Natl. Acad. Sci. USA.* 91:5740–5747.
3. Schwille, P. 2001. Fluorescence correlation spectroscopy and its potential for intracellular applications. *Cell Biochem. Biophys.* 34:383–408.
4. Fahey, P. F., D. E. Koppel, L. S. Barak, D. E. Wolf, E. L. Elson, and W. W. Webb. 1977. Lateral diffusion in planar lipid bilayers. *Science.* 195:305–306.
5. Schwille, P., J. Korlach, and W. W. Webb. 1999. Fluorescence correlation spectroscopy with single-molecule sensitivity on cell and model membranes. *Cytometry.* 36:176–182.
6. Korlach, J., P. Schwille, W. W. Webb, and G. W. Feigenson. 1999. Characterization of lipid bilayer phases by confocal microscopy and fluorescence correlation spectroscopy. *Proc. Natl. Acad. Sci. USA.* 96:8461–8466.
7. Weissman, M., H. Schindler, and G. Feher. 1976. Determination of molecular weights by fluctuation spectroscopy: application to DNA. *Proc. Natl. Acad. Sci. USA.* 73:2776–2780.
8. Petersen, N. O. 1986. Scanning fluorescence correlation spectroscopy. I. Theory and simulation of aggregation measurements. *Biophys. J.* 49: 809–815.
9. Petersen, N. O., D. C. Johnson, and M. J. Schlesinger. 1986. Scanning fluorescence correlation spectroscopy. II. Application to virus glycoprotein aggregation. *Biophys. J.* 49:817–820.
10. Skinner, J. P., Y. Chen, and J. D. Muller. 2005. Position-sensitive scanning fluorescence correlation spectroscopy. *Biophys. J.* 89:1288–1301.
11. Xiao, Y., V. Buschmann, and K. D. Weston. 2005. Scanning fluorescence correlation spectroscopy: a tool for probing microsecond dynamics of surface-bound fluorescent species. *Anal. Chem.* 77:36–46.
12. Petersen, N. O., P. L. Hoddelius, P. W. Wiseman, O. Seger, and K. E. Magnusson. 1993. Quantitation of membrane receptor distributions by image correlation spectroscopy: concept and application. *Biophys. J.* 65:1135–1146.
13. Digman, M. A., C. M. Brown, P. Sengupta, P. W. Wiseman, A. R. Horwitz, and E. Gratton. 2005. Measuring fast dynamics in solutions and cells with a laser scanning microscope. *Biophys. J.* 89:1317–1327.
14. Ruan, Q., M. A. Cheng, M. Levi, E. Gratton, and W. W. Mantulin. 2004. Spatial-temporal studies of membrane dynamics: scanning fluorescence correlation spectroscopy (SFCS). *Biophys. J.* 87:1260–1267.
15. Brinkmeier, M., K. Dorre, J. Stephan, and M. Eigen. 1999. Two-beam cross correlation: a method to characterize transport phenomena in micrometer-sized structures. *Anal. Chem.* 71:609–616.
16. Weidemann, T., M. Wachsmuth, M. Tewes, K. Rippe, and J. Langowski. 2002. Analysis of ligand binding by two-colour fluorescence cross-correlation spectroscopy. *Single Mol.* 3:49–61.
17. Schwille, P., F. J. Meyer-Almes, and R. Rigler. 1997. Dual-color fluorescence cross-correlation spectroscopy for multicomponent diffusional analysis in solution. *Biophys. J.* 72:1878–1886.
18. Bacia, K., D. Scherfeld, N. Kahya, and P. Schwille. 2004. Fluorescence correlation spectroscopy relates rafts in model and native membranes. *Biophys. J.* 87:1034–1043.
19. Proszynski, T. J., R. W. Klemm, M. Gravert, P. P. Hsu, Y. Gloor, J. Wagner, K. Kozak, H. Grabner, K. Walzer, M. Bagnat, K. Simons, and C. Walch-Solimena. 2005. A genome-wide visual screen reveals a role for sphingolipids and ergosterol in cell surface delivery in yeast. *Proc. Natl. Acad. Sci. USA.* 102:17981–17986.
20. Kahya, N., D. Scherfeld, K. Bacia, B. Poolman, and P. Schwille. 2003. Probing lipid mobility of raft-exhibiting model membranes by fluorescence correlation spectroscopy. *J. Biol. Chem.* 278:28109–28115.
21. Chiantia, S., N. Kahya, and P. Schwille. 2005. Dehydration damage of domain-exhibiting supported bilayers: an AFM study on the protective effects of disaccharides and other stabilizing substances. *Langmuir.* 21:6317–6323.
22. Magatti, D., and F. Ferri. 2001. Fast multi-τ real-time software correlator for dynamic light scattering. *Appl. Opt.* 40:4011–4021.
23. Thews, E., M. Gerken, R. Eckert, J. Zapfel, C. Tietz, and J. Wrachtrup. 2005. Cross-talk free fluorescence cross-correlation spectroscopy in live cells. *Biophys. J.* 89:2069–2076.
24. Petrov, E. P., and P. Schwille. 2005. Fluorescence correlation spectroscopy on undulating membranes. *Biophys. J.* 88:524A–525A.
25. Enderlein, J., I. Gregor, D. Patra, and J. Fitter. 2004. Art and artifacts of fluorescence correlation spectroscopy. *Curr. Pharm. Biotechnol.* 5:155–161.
26. Kim, S. A., K. G. Heinze, K. Bacia, M. N. Waxham, and P. Schwille. 2005. Two-photon cross-correlation analysis of intracellular reactions with variable stoichiometry. *Biophys. J.* 88:4319–4336.
27. Muller, B. K., E. Zaychikov, C. Brauchle, and D. C. Lamb. 2005. Pulsed interleaved excitation. *Biophys. J.* 89:3508–3522.
28. Valdez-Taubas, J., and H. R. B. Pelham. 2003. Slow diffusion of proteins in the yeast plasma membrane allows polarity to be maintained by endocytic cycling. *Curr. Biol.* 13:1636–1640.
29. Saffarian, S., and E. L. Elson. 2003. Statistical analysis of fluorescence correlation spectroscopy: the standard deviation and bias. *Biophys. J.* 84:2030–2042.